Study of the Efficiency of a Computer Code to Analyze the Performance of a Rotating Machine: Application on a Savonius Wind Turbine

Francis RAVELOSON[1] and Roger VONY[2]

[1]Faculty of Sciences

[2-]Faculty of Sciences

University Nord d'Antsiranana (UNA)

Antsiranana, Province

Madagascar

_____

ABSTRACT

The wind turbine is one of the sources of renewable energies very solicited to solve global energy problems. Among the various technologies of a rotor, that of a Savonius wind turbine is technically best suited in developing sending countries. Despite its weakness in performance, it has some advantages exploitable both on its mechanical torque and on its starting speed. In this work, we tested the effectiveness of a computer code that we designed to increase its efficiency before multiplying it. To do this, the numerical simulation of the aerodynamic performances of a vertical axis wind turbine of the Savonius type was chosen in order to validate our code. The Computational Fluid Dynamic (CFD) code, which is designed in Fortran, makes it possible to give fine predictions on the profiles of pressure fields, velocities and some aerodynamic characteristic variables of the wind turbine (moment, mechanical torque, shock wave, turbulence, ...) characterizing the performance of a rotating machine. The numerical resolution method adopted in this analysis is that of explicit finite difference. The Lax discretization scheme at two-time steps followed by addition of corrected artificial (numerical) viscosity was used. The spatiotemporal precision is in two orders, whose stability is dictated by the so-called CFL (Current Friedrich Levy) condition which imposes a constraint on the time step Δt. A detailed study of the results obtained and phenomena developed all around the blade have been made in order to draw conclusions.

Key Words: *Lax method, CFD; Savonius rotor, Vvertical axis, Wind turbine, Digital viscosity method.*
_____

1. INTRODUCTION

All the countries of the world are witnessing the serious repercussions of climate change due to the increase of carbon dioxide and other greenhouse gases caused by human activities. Electricity generation and transport are the main sectors responsible for air pollution. It is therefore more than necessary to take advantage of existing solutions to prevent damage to our planet. Natural ecosystems offer opportunities to reduce greenhouse gas emissions in a significant way and to preserve the adaptive potential of our biosphere. The use of these different sources of energy is one of the reliable solutions to significantly reduce emissions of pollutants into the atmosphere [1] both locally and globally. The wind energy is among others has certain advantages over the reduction of atmospheric pollutants because the latter is generally clean, safe and above all, it exists in unlimited quantities. Their exploitation is also a very important positive factor for developing certain region such as in urban and rural areas.

However, the main weaknesses of a wind turbine are on the irregularity of its production, the rise of its price and the weakness of its yield (especially vertical wind turbine). In addition, its production depends inevitably on climatic conditions. In order to exploit it favorably, it is therefore essential to know the characteristics of the physical phenomena encountered in the flow of fluids. To overcome this, a lot of research has been done to determine the fine structure of the flow through the blades of wind turbines to make them profitable both economically and technically. In the case of a vertical axis Savonius wind turbine, despite its weakness in performance [2], many researchers are interested in this last time. As examples, we cite some research that has been done in recent years, such as Can Kang et al. [3], Debnath and Gupta [4] in 2013 and Nilavarasan and Dheenadhayalan [5], Tian et al. [6], Frikha et al. [7] and Driss et al. [8] in 2015 or Zhang et al. [9] in 2017 who have all studied the performance of a

Savonius rotor modified with different approaches to improve its performance. The study of the influence of an angle of incidence on the performance of a rotor according to Frikha et al. [10] in 2016 and a Savonius-Savonius hybrid system from Sharma et al. [11] or Darrieus-Savonius of Dwiyantoro et al. [12] also make a good contribution this last time. In turn, RUS [13] in 2012 and recently Kang et al. [14] in 2018 used a flow guiding system to make the efficiency of a Savonius turbine profitable. One of the improvements that some researchers have been interested in lately is also the internal or external overlap of a Savonius rotor [8,15-17].

The use of very powerful CFD software such as Ansys-Fluent [3-7, 9, 10, 14, 20], SolidWorks Flow Simulation [8] or COMSOL [1] is an ideal solution in the aerodynamic field for analyze and make profitable the performances of a wind turbine since the development of computer science. However, these programs are all commercial and most developing countries have not had the means to buy them. Faced with the problems raised, the present work focuses on the study of the efficiency of a new computer code which is designed to predict the performance of a rotating machine. The generation of a mesh as well as the resolution itself are all performed on the same code. The numerical simulation in 3D will be realized with the explicit method of discretization whose diagram is that of Lax with two-time steps to increase the precision of the results. The results will be presented as well as their interpretations.

2.MATERIALS AND METHODS

In this study, we are interested in the numerical simulation of a flow of fluids around a rotor of a Savonius wind turbine. Simulations of the flow are performed in three-dimensional and unsteady with orthogonal moving mesh.

2.1 Mathematical Modeling of the Problem
Before mathematically modeling the flow of fluids, it is necessary to present the geometry model of the computational domain.

2.1.1   Geometric configuration
Savonius Wind Turbine is basically a vertical axis wind turbine named after its Finnish inventor [4]. The geometry of the conventional Savonius turbine is obtained when a cylinder is cut into two halves and the concave sections face each other and move laterally along the section plane to form a space noted e so that their parts overlap, as shown in Figure 1. In this study, the diameter and the radius of the turbine are designated respectively by D and R, while the diameter and the radius of the blade are respectively designated by d and r. The height of the turbine, the internal overlap of the blades, the diameter of the shaft and the elongation of the field are respectively denoted by H, e, a and L. The rotor size can be summarized in Table 1 below:

Table1. Geometric parameters of a Savonius wind turbine

Dimensions of Savonius Wind turbine							
D	R	H	r	e	ep	d	L
1.08m	0.54m	1.2m	0.30m	0.12m	0.005m	0.60m	1.35m

The following figures show the profile of a Savonius wind turbine, their blades and the field of study.

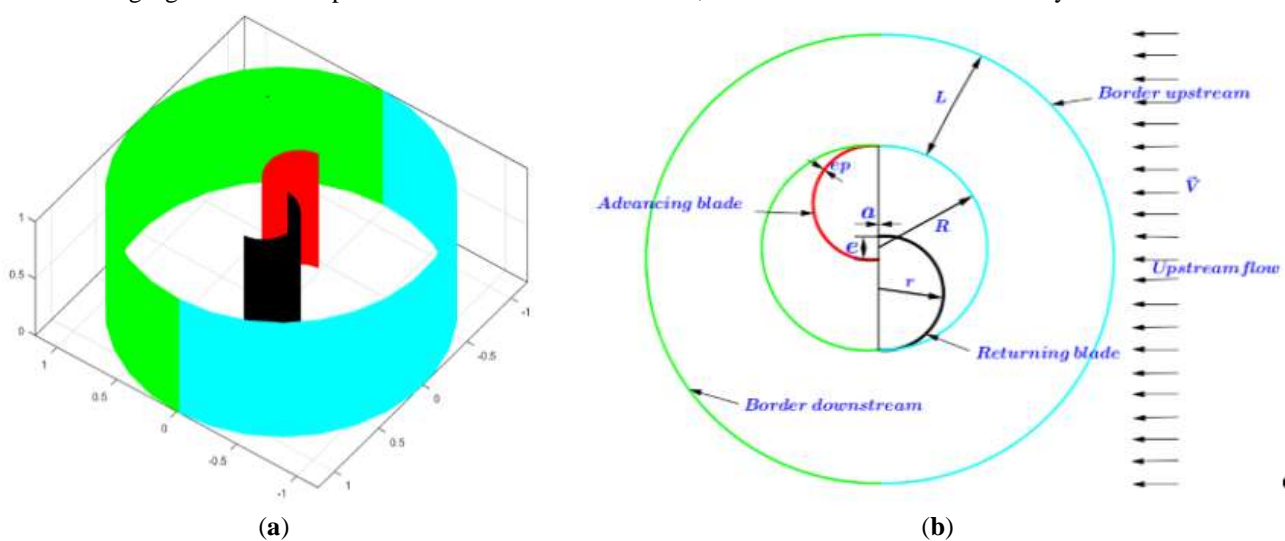(a)   (b)
Figure1. Geometric configuration (a) of the blades of a Savonius wind turbine and three-dimensional (3D) study area, (b) blade profile in bidimensional (2D) study area boundary

2.1.2   Mathematical modeling

These principles consist in realizing, at every point in the flow, the mass, momentum and energy balances, or in applying the fundamental laws of mechanics. These result in the principles of conservation of mass, momentum and energy applied to an elementary volume of matter in its movement. In the case of Newtonian fluids such as water, oil or air, a linear stress relationship provides the basic equations with sufficient accuracy [19]. Nevertheless, the equations governing the flow of fluids (continuity, momentum and energy) are among those most difficult to solve or impossible analytically. Even numerical resolution requires in many cases Rogowski and Maroński [20] simplifying hypotheses to find results without changing the phenomena. As a result, the three-dimensional, axisymmetric and unsteady flow is assumed to be non-viscous, non-heavy and no thermal conductivity. Thus, the equations governing the conservation of the mass, the momentum and the energy are respectively given by:

$$\frac{\partial \rho}{\partial t} + \vec{\nabla}(\rho.\vec{V}) = 0, \tag{1}$$

$$\frac{\partial(\rho\vec{V})}{\partial t} + \vec{\nabla}(\rho\vec{V}.\vec{V}) = -\vec{\nabla}p, \tag{2}$$

$$\frac{\partial T}{\partial t} + \vec{V}.\vec{\nabla}(T) + \frac{a^2}{c_p}\vec{\nabla}.\vec{V} = 0, \tag{3}$$

Where ρ is the density of the air; $\vec{V}$ is the velocity vector; p is the static pressure; T is the static temperature; C_p is the specific heat capacity at constant pressure; t is the time variable and a is the speed of sound.

2.1.3   Reference used

The relative references used in this study are two types, the first of which is orthogonal and pseudo-cylindrical while the second is not orthogonal but connected to the current layers. The following figures show these two landmarks.
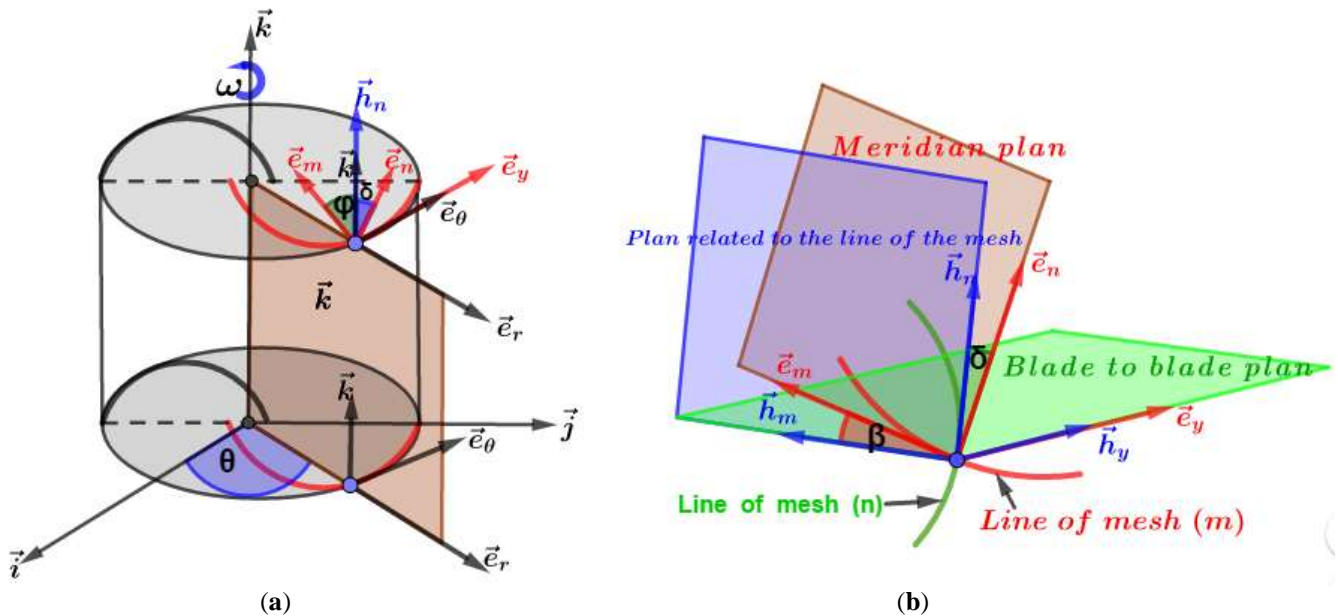

(a)   (b)

Figure2. Movable references (a) axisymmetric noted (E), (b) bound to the notched mesh (H)

The adiabatic and non-viscous flow of a compressible fluid in a rotor of a turbomachine is described by the Euler equations expressed in a pseudo-cylindrical coordinate system ($\vec{e}_m$, $\vec{e}_y$, $\vec{e}_n$) and rotating around the axis of the machine with angular velocity ω. The relative speed (W) and the absolute velocity (V) of a fluid particle remote from the axis of rotation by a distance r, are interconnected by the following relation:

$$\vec{V} = \vec{W} + \omega r \vec{e}_y, \tag{4}$$

To better analyze the physical phenomena encountered, we project afterwards the equations of motion of the fluids in another moving coordinate system denoted by (H) which is linked to the current layer. Thus, the equation of continuity, Euler and energy are written in the reference (H) as follows:

- Continuity equation :

$$\frac{\partial \rho\prime}{\partial t} = W_m \frac{\partial \rho\prime}{\partial m} + \varepsilon \frac{\partial \rho\prime}{\partial y} + W_n \frac{\partial \rho\prime}{\partial n} + \frac{\partial W_m}{\partial m} + \frac{\partial W_y}{\partial y} - tan\beta \frac{\partial W_m}{\partial y} - tan\delta \frac{\partial W_n}{\partial y} + \frac{\partial W_n}{\partial n} - W_m \left(\frac{sin\varphi}{r} + \frac{\partial \varphi}{\partial n}\right) + W_n \left(\frac{cos\varphi}{r} + \frac{\partial \varphi}{\partial m}\right), \tag{5}$$

- Conservation equation of momentum :

$$\frac{\partial W_m}{\partial t} = W_m \frac{\partial W_m}{\partial m} + \varepsilon \frac{\partial W_m}{\partial y} + W_n \frac{\partial W_m}{\partial n} + R_g \left[\frac{\partial T}{\partial m} - tan\beta \frac{\partial T}{\partial y}\right] + \frac{a^2}{\gamma}\left[\frac{\partial \rho\prime}{\partial m} - tan\delta \frac{\partial \rho\prime}{\partial y}\right] + \frac{W_y{}^2}{r} sin\varphi + W_n \left(W_n \frac{\partial \varphi}{\partial n} + W_m \frac{\partial \varphi}{\partial m}\right), \tag{6}$$

$$\frac{\partial W_y}{\partial t} = W_m \frac{\partial W_y}{\partial m} + \varepsilon \frac{\partial W_y}{\partial y} + W_n \frac{\partial W_y}{\partial n} + R_g \frac{\partial T}{\partial m} + \frac{a^2}{\gamma}\frac{\partial \rho\prime}{\partial m} + (W_y + 2U)\left(W_n \frac{cos\varphi}{r} + W_m \frac{sin\varphi}{r}\right), \tag{7}$$

$$\frac{\partial W_n}{\partial t} = W_m \frac{\partial W_n}{\partial m} + \varepsilon \frac{\partial W_n}{\partial y} + W_n \frac{\partial W_n}{\partial n} + R_g \left[\frac{\partial T}{\partial n} - tan\beta \frac{\partial T}{\partial y} \right] + \frac{a^2}{\gamma} \left[\frac{\partial \rho'}{\partial n} - tan\delta \frac{\partial \rho'}{\partial y} \right] + \frac{W_y^2}{r} cos\varphi - W_m \left(W_n \frac{\partial \varphi}{\partial n} + W_m \frac{\partial \varphi}{\partial m} \right), \qquad (8)$$

- Energy equation:

$$\frac{\partial T}{\partial t} = \frac{a^2}{C_p} \left[\frac{\partial W_m}{\partial m} - tan\beta \frac{\partial W_m}{\partial y} + \frac{\partial W_y}{\partial y} + \frac{\partial W_n}{\partial n} - tan\delta \frac{\partial W_n}{\partial y} - W_m \left(\frac{sin\varphi}{r} + \frac{\partial \varphi}{\partial n} \right) + W_n \left(\frac{cos\varphi}{r} + \frac{\partial \varphi}{\partial m} \right) \right] + W_m \frac{\partial T}{\partial m} + \varepsilon \frac{\partial T}{\partial y} + W_n \frac{\partial T}{\partial n}, \qquad (9)$$

2.2 Numerical method

The system of partial differential equations describing fluid motion can be exactly solved by a precise algorithm (direct method). This numerical exploitation makes it possible to treat the problems by transforming the continuous equations of the physics in a discrete problem on a certain domain of computation (the mesh). The generation of mesh will be obligatory before solving numerically the system of equation with the partial derivatives. In contrary of the most available codes, this one is able to generate meshes of several types whose steps are irregular or not in according to the demand.

2.2.1 Meshes generation

The physical domain of the flow is constituted by the channel comprised between two successive blades. In order to be able to correctly define the inlet and outlet conditions of the flow domain, it is extended upstream and downstream to avoid disturbances caused by boundary conditions. The rotor was placed in the axis of symmetry at a distance of 15D from the boundary of the computational domain (Fig. 3a).
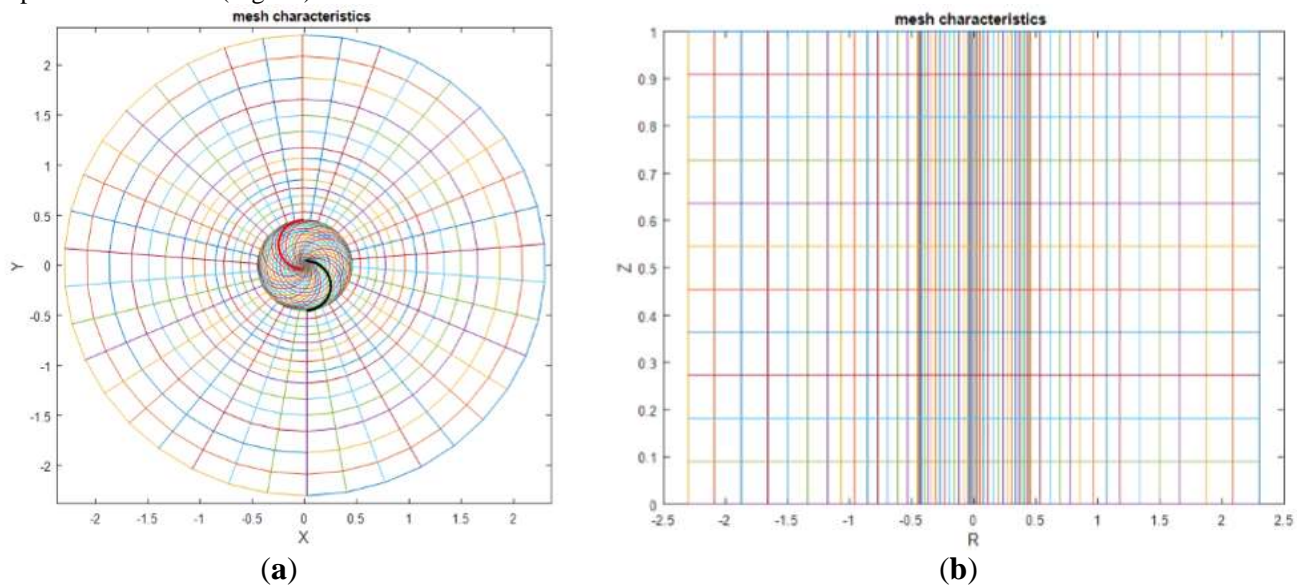

(a)   (b)

Figure3. Generated meshes (a) in the plane blade to blade, (b) in the meridian plane

The meshes in a field of study are realized by adopting a refinement of the meshes near the wall of the profile and loosened elsewhere. This mesh is chosen in order to satisfy the stability and the convergence of the results obtained but not too cumbersome during the numerical resolution. The mesh to generate is in 3D but we choose a presentation in 2D in the planes dawn with dawn and meridian to better understand it.

2.2.2 Spatial discretization of motion equations

The system of equations describing the movement of fluids is unsteady solved with explicit finite difference discretization. The numerical scheme used is the one with corrected numerical viscosity which is an extension of the Lax-Friedrichs scheme and which was introduced by Mc Donald and Couston [21]. The corrected viscosity scheme is characterized by a discretization of the spatial coordinate dependent terms using the centric schemes for the points within the computational domain and decentered inwards for the points on the boundaries.

For nodes within the flow domain, this scheme is written as follows:

$$\left[\frac{\partial \vec{Z}}{\partial S} \right]_{(l)} = \frac{\nabla S}{\Delta S (\nabla S + \Delta S)} \vec{Z}^\tau_{(l+1)} + \frac{\Delta S - \nabla S}{\Delta S \nabla S} \vec{Z}^\tau_{(l)} - \frac{\Delta S}{\Delta S (\nabla S + \Delta S)} \vec{Z}^\tau_{(l-1)}, \qquad (10)$$

For nodes on the boundaries of the flow domain, ie upstream, side-to-left, and at the bottom of the blades, this pattern becomes as follows:

$$\left[\frac{\partial \vec{Z}}{\partial S} \right]_{(l)} = \frac{\nabla S}{\Delta S (\nabla S + \Delta S)} \vec{Z}^\tau_{(l+2)} + \frac{\Delta S - \nabla S}{\Delta S \nabla S} \vec{Z}^\tau_{(l+1)} - \frac{\Delta S}{\Delta S (\nabla S + \Delta S)}, \qquad (11)$$

If the nodes are on the downstream, side-to-side and top-of-blade boundaries, it is written as follows:

$$\left[\frac{\partial \vec{Z}}{\partial S} \right]_{(l)} = \frac{\nabla S}{\Delta S (\nabla S + \Delta S)} \vec{Z}^\tau_{(l)} + \frac{\Delta S - \nabla S}{\Delta S \nabla S} \vec{Z}^\tau_{(l-1)} - \frac{\Delta S}{\Delta S (\nabla S + \Delta S)} \vec{Z}^\tau_{(l-2)}, \qquad (12)$$

In equations 10-12, $\vec{Z}$ replaces the variables to be discretized, S the spatial direction, l the index corresponding to a considered direction, ∇S and ΔS are respectively the grid steps to the left and to the right of the studied point except on the borders.

2.2.3   Temporal discretization

For temporal discretization, the variant of the Lax-Wandroff scheme followed by the addition of the corrected artificial viscosities was applied. The numerical calculation is done in three steps:

- **The first step:** Lax-Friedrich schema application (predictor):

$$\vec{Z}^{\tau+1}_{(i,j,k)} = \frac{1}{6}\left(\vec{Z}^{\tau}_{(i+1,j,k)} + \vec{Z}^{\tau}_{(i-1,j,k)} + \vec{Z}^{\tau}_{(i,j+1,k)} + \vec{Z}^{\tau}_{(i,j-1,k)} + \vec{Z}^{\tau}_{(i,j,k+1)} + \vec{Z}^{\tau}_{(i,j,k-1)}\right) + \Delta t * \left(B^{\tau}_{m(i,j,k)}\left[\frac{\partial \vec{Z}}{\partial m}\right]^{\tau}_{(i,j,k)} + \right.$$

$$\left. B^{\tau}_{y(i,j,k)}\left[\frac{\partial \vec{Z}}{\partial y}\right]^{\tau}_{(i,j,k)} + B^{\tau}_{n(i,j,k)}\left[\frac{\partial \vec{Z}}{\partial n}\right]^{\tau}_{(i,j,k)} + C^{\tau}_{(i,j,k)}\right),$$
(13)

Where, τ is the index of temporal discretization and B_m, B_y , B_n and C are variables to be discretized according to the direction considered, represented in matrix form.

- **The second step:** application of the Lax-Wendroff scheme (corrector):

$$\vec{Z}^{\tau+2}_{(i,j,k)} = \vec{Z}^{\tau}_{(i,j,k)} + \Delta t * \left(B^{\tau+1}_{m(i,j,k)}\left[\frac{\partial \vec{Z}}{\partial m}\right]^{\tau+1}_{(i,j,k)} + B^{\tau+1}_{y(i,j,k)}\left[\frac{\partial \vec{Z}}{\partial y}\right]^{\tau+1}_{(i,j,k)} + B^{\tau+1}_{n(i,j,k)}\left[\frac{\partial \vec{Z}}{\partial n}\right]^{\tau+1}_{(i,j,k)} + C^{\tau+1}_{(i,j,k)}\right),$$
(14)

This discretization scheme is of the dissipative type: it internally has damping terms, but not enough to make the calculation converge. Thus, it is necessary to add a corrected numerical viscosity which reinforces the dissipative effects and accelerates the convergence of the calculations. However, this artificial viscosity will disappear at the end of the calculation and the error it generates will not affect the accuracy of the results.

- **The third step:** adding a digital viscosity with its correction:

$$\vec{Z}^{\tau+3}_{(i,j,k)} = \vec{Z}^{\tau+2}_{(i,j,k)} - VN * \left(\vec{Z}^{\tau+2}_{(i,j,k)} - e^{*}{}_{(i,j,k)} \vec{Z}^{*}_{(i,j,k)}\right),$$
(15)

With VN is the numerical viscosity, $e^{*}{}_{(i,j,k)}$ is the numerical viscosity coefficient and $\vec{Z}^{*}_{(i,j,k)}$ is the variable obtained at the instant intermediate.

2.2.4   Schema Stability Condition

For time evolution problems, some schemes are stable provided that the time step is less than a certain critical value as a function of the height in the space. This inequality is the condition of Courant-Friedrichs-Lewy (condition CFL) which is necessary and sufficient to ensure the stability of the regime. The CFL condition varies from one equation to another as follows:

$$\Delta t < \frac{h_{(i,j,k)}}{\sqrt{3}(W+a)_{(i,j,k)}},$$
(16)

Where is the relative speed module;
    a: is the module of the speed of sound;
  $h_{(i,j,k)}$: is the minimum distance between the considered node and the six faces of the control volume.

2.2.5   Convergence of the schema

When solving the equations of fluid mechanics, the numerical methods used for an approximate problem lead to a result that is always tainted by error. But this error must be small enough for the numerical solution to tend to the real solution. Convergence is the property that guarantees that the numerical solution tends toward the exact solution of continuous equations. Thus, the error in this is very minimal especially since the results are accurate to the second orders.

2.2.6   Initial condition

The resolution of the problem of the flow of a fluid around a fixed or moving obstacle passes through the resolution of partial differential equations on a fluid domain which is bounded in particular by the solid boundary of the body. This resolution must be done from the initial moment. At the initial moment and across the section perpendicular to the main direction of flow ($\vec{e}_m$):

- The flow rate remains constant: $Q = \rho W_m A = Q_1$;
- Rothalpy remains constant: $I = \frac{W^2}{2} C_p T + \frac{\omega^2 r^2}{2} = C^{te}$;

- Following the lines of the mesh, the entropy is supposed constant (no irreversibility): $\frac{\rho}{\rho_1} = \left(\frac{T}{T_1}\right)^{\frac{1}{\gamma-1}}$.

2.2.7   Conditions to the limits

In this study, the domain of computation is based on a compromise that prejudices that the boundaries are sufficiently distant so that the disturbances generated by the boundary conditions do not influence the evolution of the physical phenomena around the profile. The boundary conditions we adopted during the numerical resolution are:

- Upstream border: the absolute speed and the angle indicating its direction are fixed. The temperature is equal to the static temperature.
- Downstream frontier: the atmospheric pressure is imposed;
- Lateral borders: condition of equality of the variables is applied;
- Solid walls: slip condition is adopted;
- In the foot and at the top of the blades: non-penetration condition is used.

3. RESULTS

Before presenting the results of our simulation, it is preferable to validate the calculation code that we have designed using a digital study already validated.

3.1 Validation of result

In this case, our code will be approved by the study of Zhang et al [9] in 2017 whose characteristics of geometry and simulation will be detailed. In this study, we analyzed the flow characteristics of non-viscous compressible fluids over those of Zhang viscous fluids. Thus, a sliding condition will be applied to the walls of the blades in our case while a condition of adhesion in his. To better compare the result to validate with the study of Zhang et al, we chose the same direction of flow. It is necessary to remember that our boundary conditions on the upstream-downstream boundaries are unsteady during the calculation.
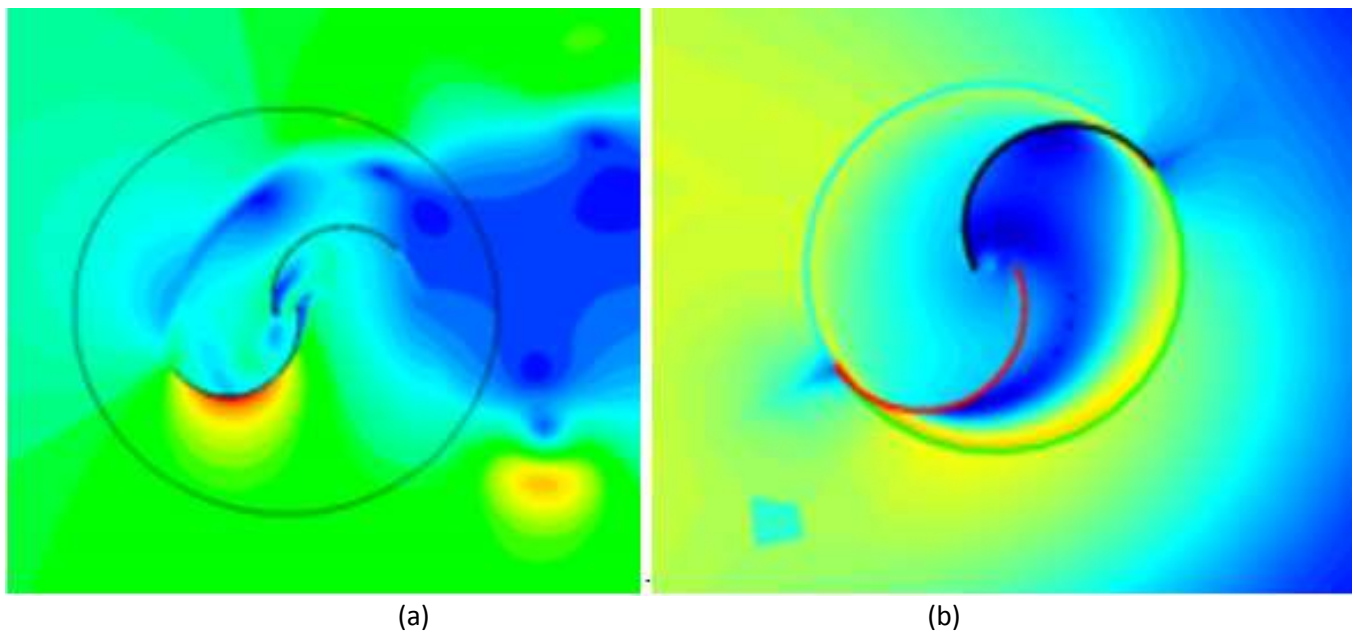

(a)   (b)

Figure4. Velocity distribution of the local flow around the Savonius rotors (a) by Zhang et al; (b) current study for same angular position.

These two results show us that the flow of fluids is slowed in the vicinity of overlapping of a rotor. There is also a difference in velocity of the flow between the concave and convex part of the two blades and especially in the vicinity of the advancing blade. At the outlet of the inter-blade channel, the velocity of the flow of the fluids decreases because of the variation of section. The extension of the field of study, which is very important in digital resolution is also a big difference. However, using the numerical method with artificial viscosity corrected leads to the resemblance of the final results.

Thus, these differences between these two studies are due on the one hand to the type of fluids to study and on the other hand to the applied boundary conditions. The fluid they studied is viscous whose adherence condition is applied to the walls of the blades and symmetricity on the sides. While a sliding condition is imposed in the case of a perfect fluid on the walls of the blades and equalities on the lateral boundaries. In addition, we applied the unsteady boundary conditions on the upstream and downstream boundaries in order to simulate the most real phenomena.

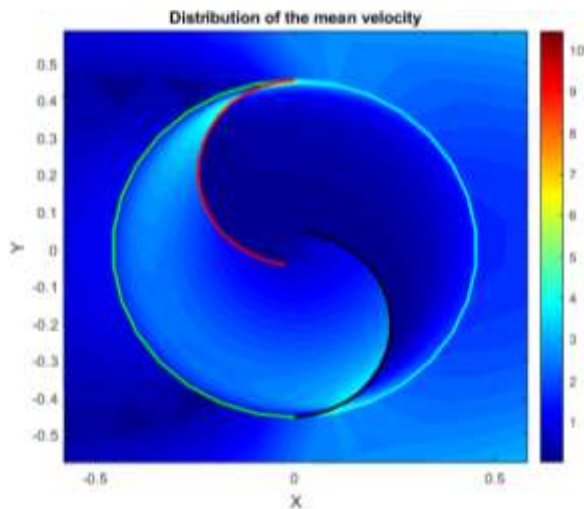### 3.2 Presentation of result

In order to better analyze the performance of our code, we decided to present the fields of relative speed and static pressure.
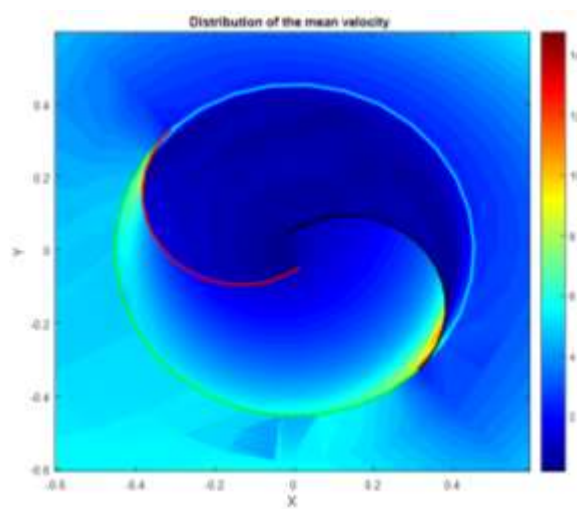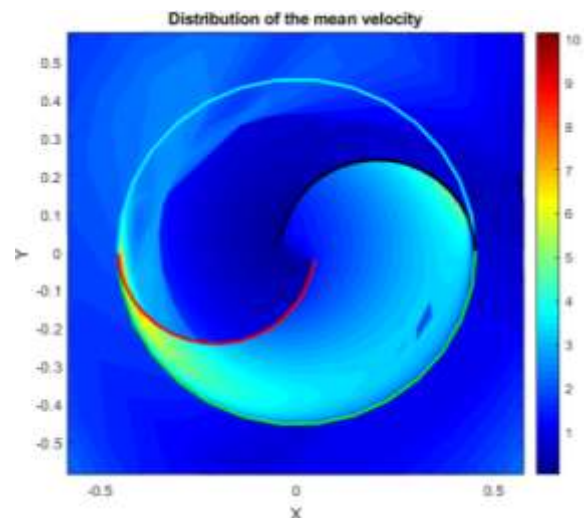

(a)

(b)

(c)

(d)

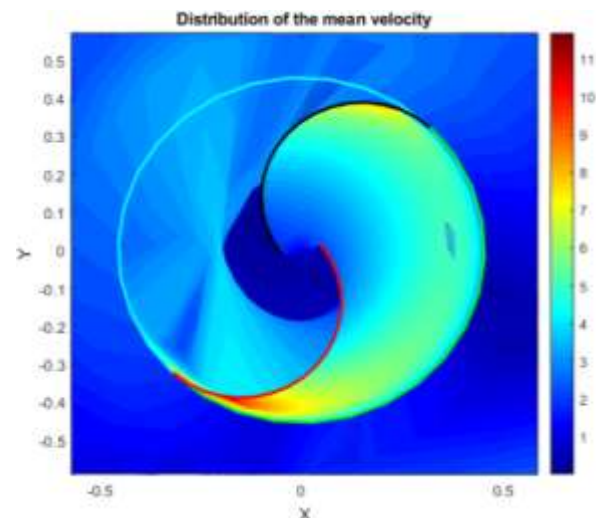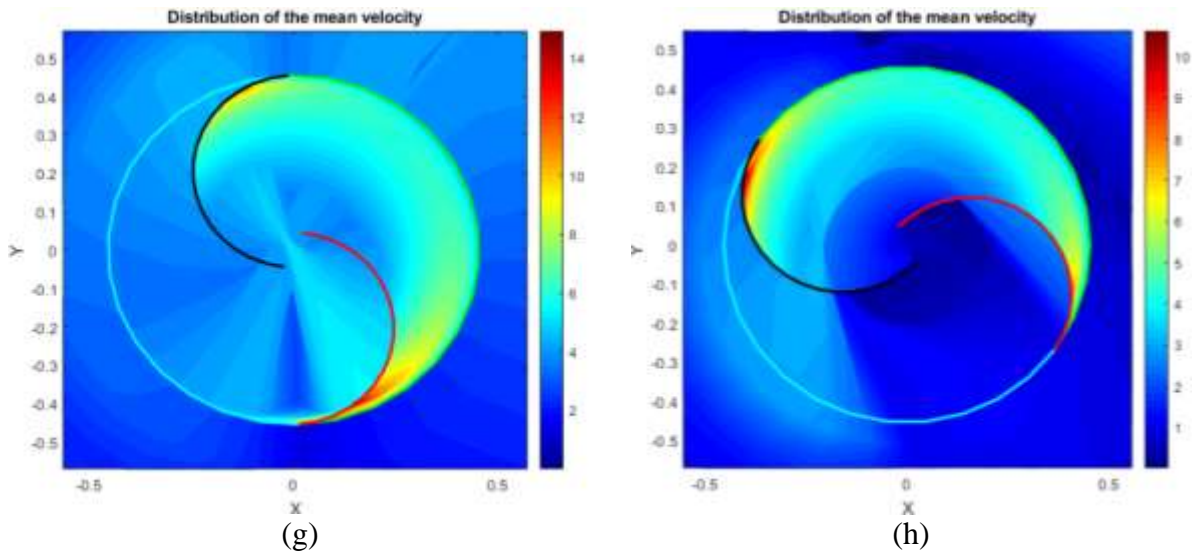(e)

(f)

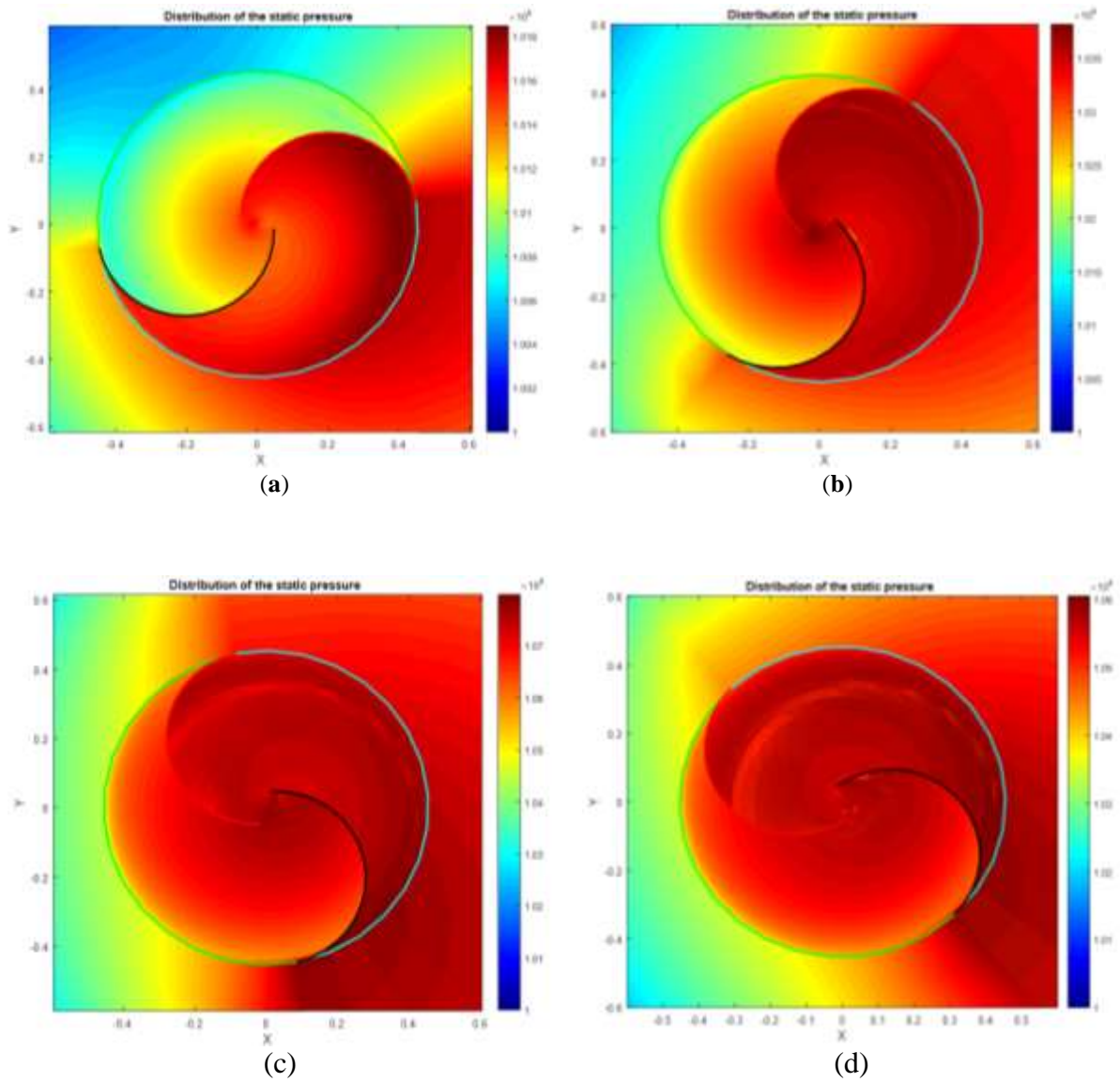(g)   (h)
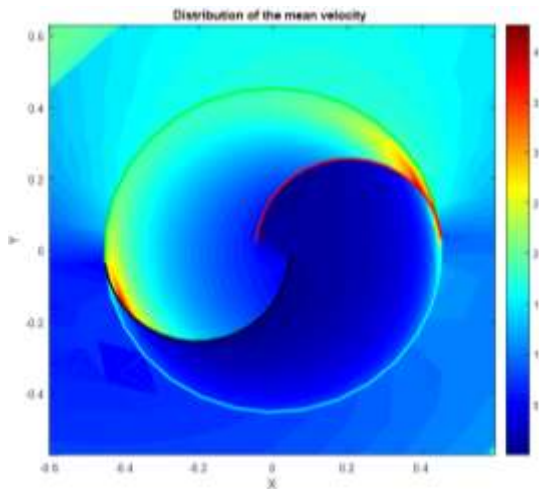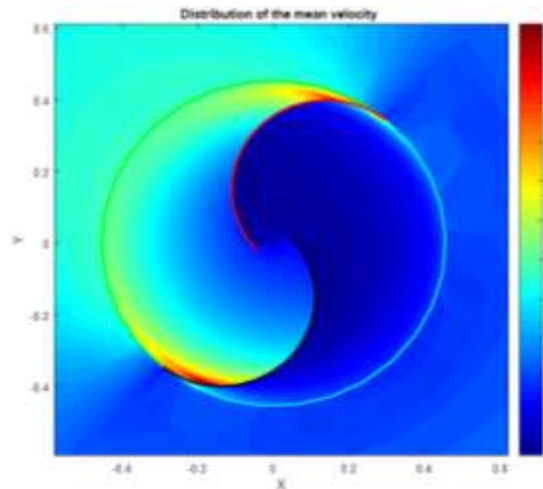
Figure 5. Relative velocity distribution of the local flow around the Savonius in rotation at different rotors angular positions

(a)   (b)

(c)   (d)
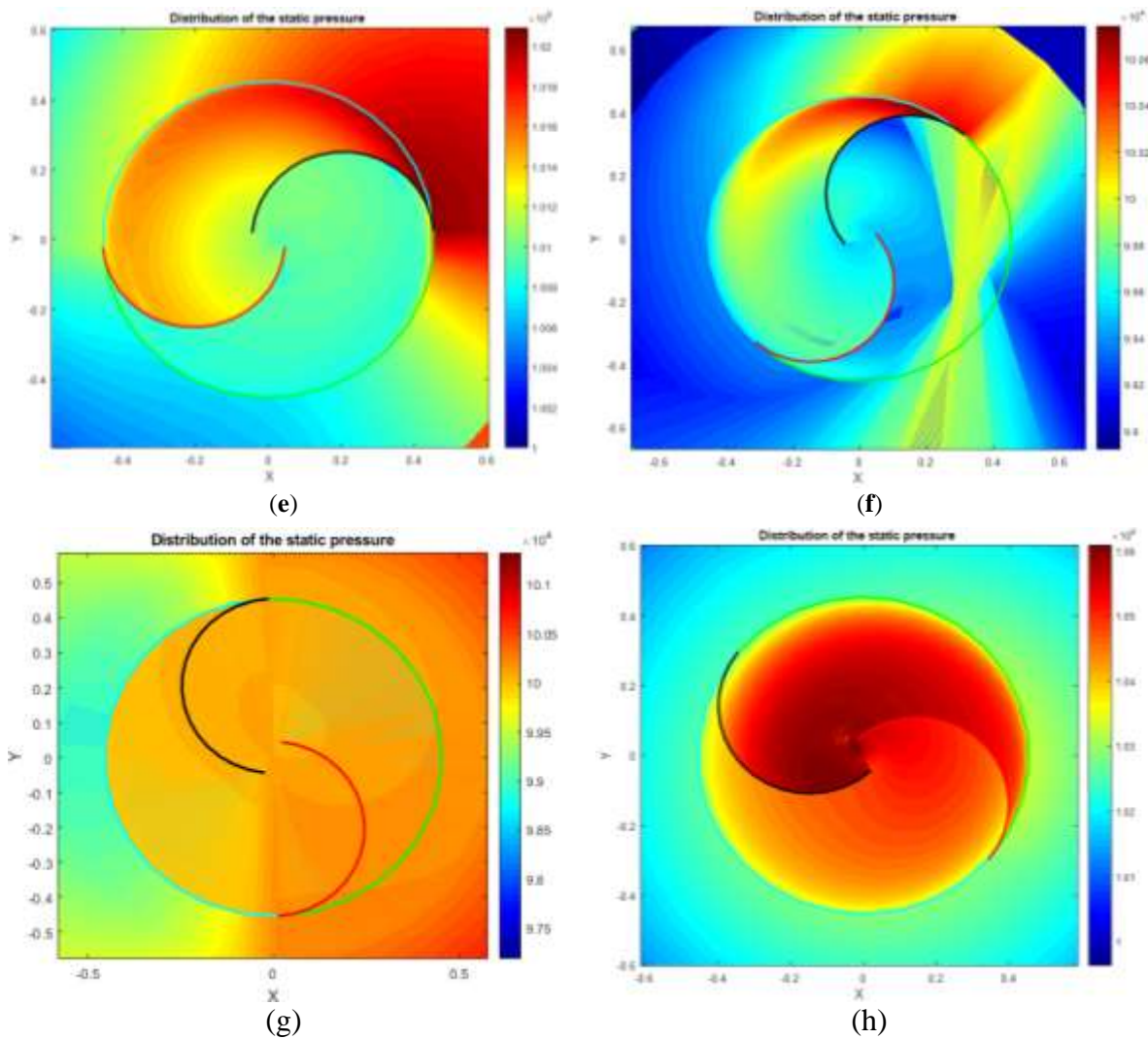
(e)

(f)

(g)

(h)

Figure 6. Static pressure distributions of the local flow around the Savonius in rotation at different rotors angular positions

4. DISCUSSION

The fields of relative velocity and static pressure through a Savonius wind turbine rotating about a fixed axis are shown in Figures 5 and 6. On both types of field, we simply took the results obtained at each 45° rotation of a rotor until it completes the complete revolution. In an unsteady study, the computation converges when the results obtained between two successive iterations are similar. Such is the case of this study; after 6 turns of a rotor all the disturbances are damped and the results are cyclic but, we want to bring much more precision. Therefore, we start extracting calculation results after 10 rotations of a rotor.

Relative velocity fields passing through a rotating Savonius wind turbine are shown in Figure 5. Calculation results across the field of study show that fluid flow is slowed down in the concave part of an advancing blade (in red) Figure 5a-e, h and accelerated in the concave part of the blade in return (black blade). This phenomenon is dominant in most areas of computation because of the overlap of a rotor that tends to slow the flow of fluids. However, this trend is less persistent when the angular position of a rotor is between 225° up to 315°. Because, in this position, it is the initially retarding blade (blade in black) which will bring the rotor in rotation; that is to say, it becomes a motor blade while the other blade (paddle in red) breaks the rotation of a rotor. That's why there is a wind turbine in Savonius where there are certain angular positions of a rotor where the torque is negative. We also observed a strong acceleration of the fluids in the vicinity of the leading edge (in the extrados) of a blade initially motor (red blade) and the proximity of edge of continuation (on the intrados) of a blade particularly resistant when the rotor angular position is between 0° to 45° and from 225° up to 360°.

The distributions of the static pressure field on each 45° rotation of a rotor are shown in Figure 6. In the vicinity of the extrados of the red blade (initially advancing blade) and the intrados of the black blade (blade initially retardant) of a rotor (Figure 6a-e), the pressure is relatively large. These are caused by the slowing down of the fluid flow in this area. At the rotor angle of 225° (Figure 6f), an area of high pressure on the concave side of the red blade of a rotor begins to decrease. This tendency is very persistent for an angular position of a rotor lying between 270° up to 315°. In addition, a sudden variation of the pressure appears in the vicinity of the leading edge of the blade by delaying (black blade). All these phenomena show us that the static pressure is inversely proportional to the speed of the flow of the fluids. This difference results on the one hand by the rotation effect of a rotor and on the other hand because of the presence of Coriolis forces and training. In addition, the rotor recovery rate has a direct influence on the performance of a Savonius wind turbine. Thus, there is an optimum value (e/d = 0.2) where the Savonius type turbine causes maximum torque.

5. CONCLUSION

This study aims to propose a new parametric design ideology to describe and optimize the vertical axis wind turbine blade. Thanks to the existence of this code and the optimization it can bring to the design of a wind turbine, certain energy problems could be solved. In order to underline some remarks and improvements that we wish to bring to future work, it seems important to remember that the Savonius wind turbine is driven by the drag whose performance is relatively low. Simulation results showed that the flow of fluids around a profile of a moving Savonius wind turbine is inversely proportional to the static pressure. Under the effects of driving forces and Coriolis, disturbances appeared near the leading and trailing edges of rotor blades. However, these disturbances are damped during the computation (resolution) thanks to the method of resolution used and the efficiency of a code of computation.

Numerical simulation of the flow of fluids in an inter-vane channel shows that the pressure downstream of the turbine is lower than that of the inlet. As a result, the wind turbine is a pressure reducing machine, which is why it is called a turbine.

The results of this code are then reliable. It must be recognized that an analysis of the pressing forces exerted on the blades of a rotating machine is a very important step in order to estimate the mechanical torque collected at the end of the shaft as well as the power obtained on a wind turbine. This is then the result of a study that we will bring in the future work to be able to propose a new geometrical configuration of a rotating machine.

ACKNOWLEDGMENT

REFERENCES

1. Andrea, A.; Antonio, E.; Alberto, M.; Calogero, O.; Flavio, T. Slotted Blades Savonius Wind Turbine Analysis by CFD. *www.mdpi.com/journal/energies* **Energies 2013, 6, 6335-6351; doi:10.3390/en6126335**.

2. Hassanzadeh, A., R.; Yaakob, O.; Ahmed, Y., M.; Ismail, A., M. Comparison of Conventional and Helical Savonius Marine Current Turbine Using Computational Fluid Dynamics. *World Applied Sciences Journal 28 (8): 1113-1119, 2013.* **DOI: 10.5829/idosi.wasj.2013.28.08.1385**.

3. Can, K.; Xin, Y.; Yuli, W. Turbulent Flow Characteristics and Dynamics Response of a Vertical-Axis Spiral Rotor. *www.mdpi.com/journal/energies* **Energies 2013, 6, 2741-2758; doi:10.3390/en6062741**.

4. Debnath, P.; Gupta, R. Flow Physics Analysis of Three-Bucket Helical Savonius Rotor at 90° Twist Angle Using CFD. *International Journal of Modern Engineering Research (IJMER), March-April. 2013, Vol.3, Issue.2, pp-739-746.*

5. Nilavarasan, T.; Dheenadhayalan, J. Computational Investigation of Fluid Dynamic Aspects of Classical and Modified Savonius Wind Turbines. *International Journal of Core Engineering & Management (IJCEM);* Volume 1, Issue 12, March 2015, pp. 102-109.

6. Wenlong, T.; Baowei, S.; James H., V.; Parakram, P. Computational Fluid Dynamics Prediction of a Modified Savonius Wind Turbine with Novel Blade Shapes. *www.mdpi.com/journal/energies* **Energies 2015, 8, 7915-7929; doi:10.3390/en8087915**.

7. Sobhi, F.; Zied, D.; Hedi, K.; Mohamed, S., P. Study of the Computational Domain Effect on the Aerodynamic Structure Around a Savonius Wind Rotor. *International Journal of Fluid Mechanics & Thermal Sciences*. Vol. 1, No. 2, 2015, pp. 20-24; **doi: 10.11648/j.ijfmts.20150102.11**.

8. Zied, D.; Olfa, M.; Slah, D.; Makram, M.; Mohamed, S., P. Numerical Study of an Unconventional Savonius Wind Rotor with a 75° Bucket Arc Angle. *American Journal of Mechanical Engineering, 2015, Vol. 3, No. 3A, 15-21.* **DOI:10.12691/ajme-3-3A-3**.

9. Baoshou, Z.; Baowei, S.; Zhaoyong, M.; Wenlong, T.; Boyang, L.; Bo, L. A Novel Parametric Modeling Method and Optimal Design for Savonius Wind Turbines. *www.mdpi.com/journal/energies* **Energies 2017, 10, 301; doi :10.3390/en10030301**.

10. Sobhi, F.; Zied, D.; Hedi, K.; Mohamed, S., P. Incidence Angle Effect on the Turbulent Flow around a Savonius Wind Rotor. *American Journal of Energy Research, 2016, Vol. 4, No. 2, 42-53.* **DOI:10.12691/ajer-4-2-3**.

11. Sharma, K., K.; Gupta, R.; Biswas, A. Performance Measurement of a Two-Stage Two-Bladed Savonius Rotor. *International Journal of Renewable Energy Research, K.K. Sharma et al., Vol.4, No.1, 2014*.

12. Bambang, A., D.; Triyogi, Y.; Vivien, S. Structural Design Optimization of Vertical Axis Wind Turbine Type Darrieus-Savonius. *ARPN Journal of Engineering and Applied Sciences, January 2016 Vol. 11, No. 2, 1073-1077.*

13. RUS, L., F. Experimental study on the increase of the efficiency of Vertical Axis Wind Turbines by equipping them With Wind Concentrators. *Journal of Sustainable Energy, March, 2012, Vol. 3, No. 1, 30-35.*

14. Can, K.; Wisdom, O.; Chen, P.; Ziwen, Z. Upstream Flow Control for the Savonius Rotor under Various Operation Conditions. *www.mdpi.com/journal/energies* **Energies 2018, 11, 1482; doi:10.3390/en11061482**.

15. Zied, D.; Ali, D.; Mohamed, S., P. Evaluation of the Savonius Wind Rotor Performance for Different External Overlap Ratios. *International Journal of Fluid Mechanics & Thermal Sciences. Vol. 1, No. 1, 2015, pp. 1-6.* **doi: 10.11648/j.ijfmats.20150101.11**.

16. Sharma, K., K.; Gupta, R. Speed Variation in Savonius Rotors with Respect to Overlap. *International Review of Applied Engineering Research.* ISSN 2248-9967 Volume 4, Number 3 (2014), pp. 233-240.

17. Zied, D.; Ali, D.; Mohamed, S., P. Experimental investigation of the external overlap ratios effect on the performance of the Savonius wind rotor. *21ème Congrès Français de Mécanique. Bordeaux, 26 au 30 août 2013*.

18. Larin, P.; Aygun, C.; Paraschivoiu, M. CFD based analysis of Savonius turbine in synergy with flow on top of a building. *EIC Climate Change Technology Conference 2015*, **Paper Number 1570050033**.

19. Abali, B., E. An Accurate Finite Element Method for the Numerical Solution of Isothermal and Incompressible Flow of Viscous Fluid. *www.mdpi.com/journal/fluids* **Fluids 2019, 4, 5; doi:10.3390/fluids4010005**.

20. Krzysztof, R.; Ryszard, M. CFD Computation of The Savonius Rotor. *Journal of Theoretical and Applied Mechanics 53, 1, pp. 37-45, Warsaw 2015*; **DOI: 10.15632/jtam-pl.53.1.37**.

21. Hireche, O. ; Abidat, M. ; Merahi, L. ; Azzi, A. Etude de l'Ecoulement Tridimensionnel dans un Rotor d'une Turbine Semi-axiale. *Rev. Energ.* Ren. Vol. 2 (1999) 51 - 60.